Development of fine-tuned top-down mass spectrometry strategies in the chromatographic time scale (LC-TD-MS) for the complete characterization of an anti EGFR single domain antibody-drug conjugate (sdADC)

Rania Benazza, Léa Letissier, Greg Papadakos, Jen Thom, Hélène Diemer, Graham Cotton, Sarah Cianférani, Oscar Hernandez Alba

Development of top-down mass spectrometry strategies in the chromatographic timescale (LC-TD-MS) for the extended characterization of an anti-EGFR single-domain antibody-drug conjugate (sdADC) in both reduced and non-reduced forms.

Rania Benazza[1, 2†], Léa Letissier[1, 2†], Greg Papadakos[3], Jen Thom[3], Helene Diemer[1, 2], Graham Cotton[3], Sarah Cianférani[1, 2] and Oscar Hernandez-Alba[1, 2*]

[1] Laboratoire de Spectrométrie de Masse BioOrganique, IPHC UMR 7178, Université de Strasbourg, CNRS, 67087 Strasbourg, France
[2] Infrastructure Nationale de Protéomique ProFI—FR2048, 67087 Strasbourg, France
[3] Almac discovery, Edinburgh Technopole, Milton Bridge, Penicuik, Scotland, EH26 0BE, United Kingdom

ABSTRACT: Even though mAbs have attracted the biggest interest in the development of therapeutic proteins, next generation of therapeutics such as single-domain antibodies (sdAb) are propelling an increasing attention as new alternatives with appealing applications in different clinical areas. These constructs are small therapeutic proteins formed by a variable domain of the heavy chain of an antibody with multiple therapeutic and production benefits compared to their mAb counterparts. These proteins can be subjected to different bioconjugation processes to form single-domain antibody-drug conjugates (sdADC) and hence increase their therapeutic potency, and, akin to other therapeutic proteins, nanobodies and related products require dedicated analytical strategies to fully characterize their primary structure prior to their release to the market.

In this study we report for the first time on the extensive sequence characterization of a conjugated anti-EGFR 14 kDa sdADC by using state-of-the-art top-down mass spectrometry strategies in combination with liquid chromatography (LC-TD-MS). Mass analysis revealed a highly homogeneous sample with one conjugated molecule. Subsequently, the reduced sdADC was submitted to different fragmentation techniques namely higher-energy collisional dissociation (HCD), electron-transfer dissociation (ETD), and electron transfer higher-energy collision dissociation (EThcD) allowing to unambiguously asses the conjugation site with 24 diagnostic fragment ions and 85% of global sequence coverage. The sequence coverage of the non-reduced protein was significantly lower (around 16%), however the analysis of the fragmentation spectra corroborated the presence of the intra-molecular disulfide bridge along with the localization of the conjugation site.

Altogether, our results pinpoint the difficulties and challenges associated to the fragmentation of sdAb derived formats in the LC time scale due to their remarkable stability as a consequence of the intramolecular disulfide bridge. However, the use of complementary activation techniques along with identification of specific ion fragments allow an improved sequence coverage, the characterization of the intramolecular disulfide bond, and the unambiguous localization of the conjugation site.

INTRODUCTION

Monoclonal antibodies (mAbs) have changed the paradigm of cancer treatment over the last decades with more than 170 approved mAbs worldwide, and more than 200 of mAb biotherapeutics entering clinical studies per year since 2021.[1] However, in oncology, mAbs can encounter tumor resistance mechanisms and their large size comprises penetration into solid tumours, limiting their therapeutic efficacy. Thereby, efforts in protein engineering have been focused on the conception of next generation of biotherapeutics to widen their therapeutic applications. One of the

most promising therapeutics along with bi-specific antibodies (bsAbs), are single-domain antibodies (sdAb), also known as heavy chain variable domain (VHHs) or nanobodies (originally trademarked in 2003 by Ablynx). This new class of therapeutics have gained increased attention with currently three approved formats on the market[2] and around 37 nanobody candidates undergoing clinical trials so far.[3]

SdAbs derive from the naturally occurring heavy-chain antibodies (HcAbs) in camelids.[4] They are constituted of four relatively constant framework regions along with the three complementarity-determining regions (CDRs) responsible for antigen binding. Thereby, nanobodies are substantially small-sized proteins (~15 kDa) with appealing advantages against their mAb counterparts, *i.e.* better tissue penetration,[5–8] the possibility to bind clefts and cavities of target antigen,[9,10] exhibit lower toxicity and immunogenicity,[11,12] enhanced solubility,[13] and stability,[14] and lower structural heterogeneity. Furthermore, production of sdAbs can be carried out in low-cost systems like *E. coli*[15] or yeast,[16] reducing the overall production cost. For all these reasons, sdAbs have found their way into different applications such as infectious diseases,[17] cancer therapy,[18] and central nervous system (CNS) disorders.[19] Akin to mAbs, nanobodies can be subjected to covalent modifications allowing incorporation of cargo molecules with different properties allowing the use of conjugated nanobodies as drug carriers[20] (single domain antibody-drug conjugate, sdADC) or imaging probes.[21] Similar to other biotherapeutic proteins, the primary structure of sdAbs, and sdADCs has to be thoroughly assessed prior to their commercialization including sequence assessment, identification of post-translational modifications, and the precise localization of the position of the cargo molecules (for conjugated formats) through the development of tailored analytical methods.

The development of complementary activation techniques and their subsequent implementation in last generation high resolution MS platform has paved the way for the development of analytical workflows envisaging protein sequencing at the intact level, *i.e.*, without any prior enzymatic digestion. These strategies are encompassed under the term top-down mass spectrometry (TD-MS) and have been applied to a large variety of biomolecules among which, membrane proteins,[22–25] histones,[26–28] and oligonucleotides.[29–31] MAbs, and derived products such as antibody drug conjugates (ADCs) have also been subjected to TD-MS studies, mainly due to the advent of complementary fragmentation techniques. In most of the cases, a limited proteolysis is performed followed by a reduction step to downsize the mAb-derived protein scaffold,[32–41] and thus mitigating the challenges associated to the fragmentation of 150 kDa proteins with several chains and multiple inter-, and intra-molecule disulfide bridges. However, several examples of TD-MS studies of mAbs,[42–50] and ADCs[51,52] can be found in the literature, illustrating the potential of these methods in the characterization of biotherapeutics at the intact level. More particularly, Loo and coworkers combined ECD and HCD fragmentation (EChcD) to perform TD-MS on one mAb and its conjugated ADC under native conditions,[51] reaching an overall sequence coverage of 70% of both compounds with specific fragment ions allowing the assessment of intramolecular disulfide bridges and 58% of payload conjugation sites.

Despite the numerous publications showcasing the advantages of TD-MS workflows for intact protein sequencing, it is worth to stress that sdAbs have been scarcely characterized using these strategies, while there is not previous studies using MS-based approaches to elucidate the bioconjugation site of sdAb derived formats such as single-domain antibody drug conjugates (sdADC) at the intact level. In 2010, Resemann *et al.* performed the *de novo* sequencing of a 13 kDa nanobody using a TD-MS assisted bottom up (BU) approach.[53] In this case, the fragmentation of the intact nanobody was performed with MALDI in-source decay matrix assisted laser desorption ionization (MALDI-ISD) with two different matrix compositions in order to favor fragmentation of both protein termini, and thus provide an extended protein sequence characterization. A more recent study published by Macias *et al.* applied ultraviolet photo-dissociation (UVPD) activation to fragment three different nanobody-antigen pairs.[54] This experiment was conducted under native MS conditions (nMS) with the main purpose of inferring structural insights onto the quaternary structure of nanobody-antigen pairs from their corresponding UVPD fragmentation spectra. In this context, the fragmentation of the apo-, and holo- forms of the nanobodies were compared to detect significant fragmentation differences upon antigen binding. According to the reported results, the fragment ions originated under both conditions pinpointed a fragmentation suppression located at the antigen-nanobody interfaces leading to the conclusion that UVPD-based native TD-MS can significantly contribute to determine nanobody's paratopes.

As evidenced by the scarce number of reported studies, nanobodies, and their conjugated counterparts have not been extensively studied with TD-MS workflows for their primary structure characterization. Moreover, both studies used direct infusion without providing further evidence

demonstrating the suitability of the TD-MS strategies in the characterization of sdAbs in the chromatographic time scale. Here we report for the first time on the characterization of an in-house sdADC using a tailored reversed-phase liquid chromatography top-down mass spectrometry (RPLC-TD-MS) strategy based on higher energy collision induced dissociation (HCD), electron transfer dissociation (ETD), and Electron Transfer/Higher-Energy Collision Dissociation (EThcD). The experimental conditions of each individual activation technique were optimized to improve the fragmentation yield of the peptide backbone, highlighting the advantages/limitations of each fragmentation technique in terms of overall sequence coverage, localization of the conjugation site, and the identification of signature fragment ions to determine the presence of the intra-molecular disulfide bridge. Overall, this study provides insights about the suitability of LC-TD-MS strategies in the characterization of the primary structure of next generation sdAbs, and sdADCs biotherapeutics showing the challenges related with the sequencing of this type of therapeutics in the presence of the intramolecular disulfide bond.

MATERIAL AND METHODS

Chemicals and reagents

All buffers and the chemicals used for the protein purification and functionalization were purchased from Merck. *E. Coli* cells. Chitin affinity chromatography resin were purchased from NEB, Luria-Bertani (LB) media, ampicillin (AMP), and isopropyl β-D-1-thiogalactopyranoside (IPTG) were purchased form MelfordAlexa Fluor™ 488 C5 Maleimide (AF488) was purchased from Thermo Fisher and 5 ml HiTrap desalting columns from Cytiva.

All chemicals were purchased from Sigma-Aldrich (France): acetonitrile (ACN), ammonium acetate ($AcNOH_4$), dithiothreitol (DTT) and trifluoroacetic acid (TFA). RapiGest™ reagent was purchased from Waters (France) and trypsin from Promega (France). All aqueous solutions were prepared with ultra-pure water system (Sartorius, Göttingen, Germany). LockMass and RDa Calibrant solutions used on the BioAccord Mass Spectrometer were obtained from Waters (Manchester, UK) and the calibration solution used on the Eclipse Mass Spectrometer was a Pierce FlexMix from Thermo Fisher (France). The anti-EGFR nanobody was prepared at Almac Discovery (Scotland, UK).

Anti-EGFR production, expression, purification and conjugation

sdAb preparation and thiol functionalization — The anti-EGFR VHH 7C12 cloned to the N-terminus of a GyrA intein-chitin binding domain fusion, was expressed in *E. coli* cells and captured on chitin beads as previously described.[55]

The 7C12 intein fusion protein was then cleaved by overnight incubation at room temperature with 200 mM cysteamine in 200 mM NaCl, 50 mM sodium phosphate buffer, pH 6.9, to generate the corresponding C-terminal thiol-functionalized 7C12 protein. Cysteamine excess was further eliminated by size-exclusion chromatography (**Figure S1**).

sdAb conjugation— To conjugate to the C-terminal thiol group of 7C12 (generated by cysteamine cleavage of the precursor intein-fusion protein and referred to as the C-terminal cysteamine thiol), the purified protein was incubated with a 4-fold molar excess of Alexa Fluor 488 maleimide dye at room temperature for 1h. The excess dye was removed using a 5 mL HiTrap desalting column equilibrated in PBS, pH 7.4. , The labelling was confirmed by SDS-PAGE and ESI-TOF MS (Bruker Daltonics) The protein concentration and the degree of labelling were calculated according to the AF488 Thermo Fisher manual using the molar extinction coefficient of the protein.

Top-down MS experiments

LC-TD-MS analysis—a Dionex Ultimate 3000 LC system was used to inject between 1, and 3 µg of samples through an Agilent Zorbax 300 SB-C8 (2,1 x 50 mm, 1,8 microns) at 60°C. The solvent system consisted of 0.1% TFA in water (solvent A) and 0.1% TFA in acetonitrile (solvent B). Elution was performed at a flow rate of 200 µL/min from 20% to 65% of B for 7 minutes. The LC was hyphenated to an Orbitrap Tribrid Eclipse MS (Thermo Fisher Scientific) equipped with ETD, HCD, ETD, and EThcD options. For all experiments, the spray voltage was set to 3.4 kV, and the ion transfer tube temperature at 320 °C.

The MS scans were acquired in profile mode at a resolution of 60 000, the AGC target was 4.10^5 and the maximum of injection time 100 ms on a range of [350-4000] *m/z*. The MS/MS scans were also recorded in profile mode with a resolution of 120 000, the AGC target was 5.10^5 and the maximum injection time was 200 ms. Mass range of [180-2000] *m/z* with an isolation width of 2 *m/z* were selected for all analysis except for non-reduced sdADC where isolation was performed in the Ion Trap with an isolation width of 10 *m/z* and with a mass range of [180-4000] *m/z*. All the fragmentation spectra were recorded with 10 microscans to improve the signal quality. For HCD fragmentation, the ions were accelerated under a constant N_2 pressure of 8 mTorr. For performing ETD, anionic fluoranthene radicals were generated in the source region of the instrument. For EThcD ex-

periments, fragment ions resulting from the radical fragmentation were supplemented with an additional acceleration voltage to dissociate the non-covalent interactions between fragments. Each fragmentation conditions were applied in individual experimental analysis.

Data analysis— the MS/MS spectra were deconvoluted with Xtract algorithm on FreeStyle software, using a S/N of 3, a fit factor of 70% and a remainder threshold of 25%. The deconvoluted masses were matched to the protein sequence using Prosight Lite software with a 10-ppm ion tolerance. For each fragmentation method the type of generated ions was considered, namely *b/y* in the case of HCD, *c/z* in the case of ETD, and *b/y* and *c/z* in the case of EThcD. The C-terminus of the protein was modified with a cysteamination, thus the addition of the cysteamine mass was considered on this position. Since the bioconjugation was performed through the specific thiol-maleimide reaction, both Cys22, and Cys96 along with the C-terminus cysteamine group was considered as putative conjugation sites. All the different experiments were recorded in triplicate. Only fragment ions observed at least in two out of three replicates were considered on the final sequence coverage.

To assign the internal fragments, ClipsMS software was used by fixing the parameters as follows: terminal fragments error at 10 ppm and internal fragments error both at 5 ppm with the smallest internal fragment size at 5 AA. The cysteamine and AF488 modifications were considered as localized modifications after confirming their position by matching terminal ions with ProSight Lite. All the raw data along with matched fragments are publicly available in the jPOST repository under accession numbers PXD058380 (ProteomeXchange), and JPST003493 for jPOST.[56]

RESULTS

Intact mass analysis using SEC-nMS

Our in-house sdADC was firstly analyzed using SEC-nMS coupling to determine the experimental mass of the protein, the drug load distribution (DLD), and average drug-to-antibody ratio (avDAR) after conjugation with the surrogate cytotoxic payload molecule AF488 (**Figure 1A,B**). The SEC-UV chromatogram reveals a major peak at ~3.88 min corresponding to the monomeric sdADC with an experimental mass of 14 145.7 ± 0.1 Da that can be assigned to the sdAb conjugated to one AF488 molecule (**Figure 1B**). A minor peak is also observed at ~4.50 min corresponding to a fragmented moiety of the AF488 (**Figure S2**). According to this result, the conjugation of the sdAb was complete, leading to an avDAR of 1. This result is in line with the SDS page analysis where the conjugation of the AF488 molecule was confirmed upon UV visualization of the reduced sdADC (**Figure S3**). However, the resolution, and mass accuracy of the SEC-nMS coupling allowed to confirm that the experimental mass of the protein corresponded to the D1 population of the sdADC with a disulfide bridge, suggesting that the integrity of the intra-molecular linkage between both cysteine residues has been maintained during the conjugation process.

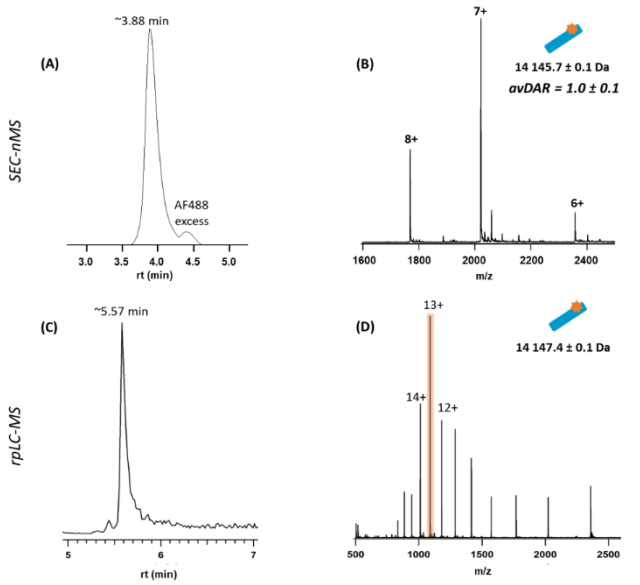

Figure 1: Analysis of unreduced sdADC in native conditions using SEC-nMS (top panels) and the reduced form in denaturing conditions using rpLC-MS (bottom panels). **(A)** SEC-UV chromatogram. **(B)** MS spectra corresponding to the eluted sdADC in native conditions. **(C)** Total ion chromatogram of the reduced sdADC showing one species at ~5.57 min. **(D)** MS spectra of the reduced sdADC in denaturing conditions. The peak highlighted in orange was selected for further TD-MS experiments.

TD-MS for the sequence characterization and conjugation site identification of the sdADC

Recent studies have shown the benefits of TD-MS for the characterization of protein modifications through the direct fragmentation of intact proteins,[26,27,57–61] although the sequence coverage is significantly reduced when dealing with large molecular ions (> 30 kDa).[33,41,49,62,63] Taking into account the relative small size of the sdADC, it seems to be the suitable candidate to be subjected to TD-MS workflows in order to perform sequence assessment, along with the localization of the AF488 molecule in the protein backbone. Since the sequence coverage of the proteins significantly di-

minishes with the presence of intra-molecular disulfide bonds,[64–66] the conjugation site and the sequence confirmation of the sdADC were carried out upon reduction of the cysteine residues (see material and method section, **Figure 1C, D**). The reduction of the disulfide bridge along with the use of chaotropic agents disrupt the secondary and tertiary structures of the protein, allowing the accommodation of higher number of protons during the ESI process, and thus increasing the overall net charge state of the molecular ions. One major peak centered at ~5.57 min is observed in the chromatogram profile of the sdADC. The charge envelop was centered at the 13+ charge state, and the corresponding experimental mass associated to the main peak was 14 147.4 ± 0.1 Da, in line with the reduced form of the sdADC bearing one AF488 molecule (+ 757.1182 Da) **(Figure 1D)**.

Subsequently, the reduced sdADC was analyzed using rpLC-TD-MS using different activation techniques such as HCD, ETD, and EThcD. Optimization of the fragmentation reaction and the charge state of the precursor molecular ions were conducted on the unconjugated sdAb as a reference sample. Three charge states (12+, 13+ and 14+) were selected for HCD fragmentation combined with collision energies from 10 to 30% NCE (**Figure S4**). Interestingly, fragmentation of the 12+ precursor ion gave rise to the largest number of fragments leading to a sequence coverage of 31% (*versus* 23 for 12+ and 14+, respectively, **Figure S4A**). Moreover, the activation energy was also optimized, reaching 35% of sequence coverage with 20% NCE (**Figure S4B**).

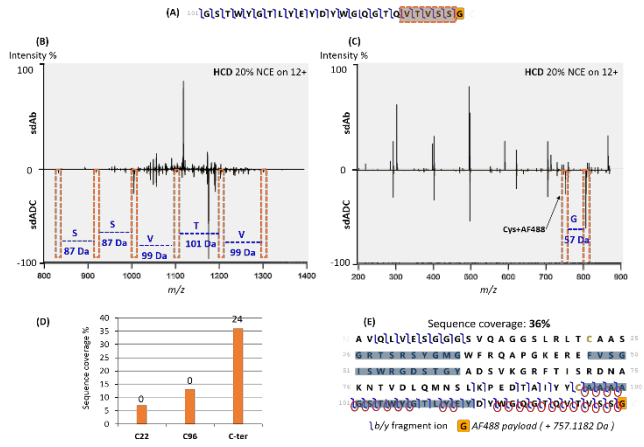

Figure 2: TD-MS experiments of reduced sdADC. (**A**) Sequence coverage of sdADC C-terminal site upon 20% NCE HCD.(**B and C**) MS/MS spectra upon 20% NCE HCD fragmentation of sdAb (top) and sdADC (bottom) showing new fragment ions in the case of the sdADC corresponding to the AF488 modification. (**D**) Histogram representing the sequence coverage and diagnostic fragment ions with the different conjugation positions. (**E**) Fragmentation map of matched *b/y* ions with the sdADC sequence. AF488 modification is outlined in an orange frame, specific fragments are depicted with red circles, and CDRs are highlighted with light blue.

The optimized fragmentation conditions were applied to the sdADC. Overall, similar fragmentation spectra of sdAb, and sdADC were obtained. However, pair comparison analysis between both spectra revealed a series of singly charged fragment ions in the sdADC spectrum that were not detected in the sdAb fragmentation pattern (**Figure 2B and 2C**) covering the 500-1400 *m/z* range. Upon calculation of the mass difference between each consecutive singly-charged ion, it was concluded that those ions corresponded to the fragmentation of the five last residues of the C-terminal side of the sdADC (VTVSSG, **Figure 2A**). Additionally, one ion at 776.165 *m/z* value was observed, corresponding to the AF488 molecule conjugated to the cysteamine residue. According to these signature ions, the conjugation of the surrogate cytotoxic payload molecule occurred on the thiol group of the cysteamine residue located in the C-terminal side of the protein.

To further strengthen this result, the variation of the sequence coverage of the sdADC as a function of the AF488 position was assessed (**Figure 2D, and S5**). Since the conjugations strategy relied on the site selective maleimide-thiol reaction, the fragment ions were matched with three different sdADC sequences containing the AF488 molecule at position Cys22, Cys96, and cysteamine 125. Thus, fragment ion matching with the conjugation site located at position Cys22, and Cys96 led to a poor sequence coverage of 7, and 13% respectively with no *b*-ions containing the aforementioned conjugated cysteine residues (**Figure 2C and S5**). Conversely, the sequence coverage rose to 36% when the conjugated molecule was located at the C-terminal side (cysteamine conjugation), providing 24 diagnostic *y*-fragment ions of the position of the AF488 molecule in the cysteamine thiol group (**Figure 2D, E**). Overall, these results are in line with the singly-charged diagnostic fragments observed upon spectra comparison between the conjugated and naked sdAb, thus leading to the unambiguous conclusion that the conjugation of the sdADC was selectively performed in the C-terminal side. This result was in line with data obtained through peptide mapping analysis. Upon digestion of the sdADC, only one AF488-bound peptide was found corresponding to the peptide covering the 117-125 region of the protein (**Figure S6**). Combination of TD-MS, and peptide mapping data clearly corroborates the selectivity of the bioconjugation strategy used to modify the initial sdAb.

Benefits of ETD and EThcD for extended sdADC sequencing

Although the conjugation site is perfectly localized with the sole use of HCD, the fragmentation yield remains relatively low for a 14 kDa protein (36%). In order to provide a more extensive sequence characterization, the use of complementary activation techniques such as ETD, and EThcD were also performed. These two techniques, along with UVPD, have been shown to provide higher sequence coverage in comparison to collision-based fragmentations, covering in a more efficient manner the interior regions of protein backbones.[32,33,35,38,67]

ETD, and EThcD reaction conditions were chosen from the optimal conditions resulting from the fragmentation of reduced sdAb (**Figure S7, S8**). Thus, the optimal ETD reaction time was set to 4 ms whereas 25% of NCE was supplemented to ETD reaction in the case of EThcD fragmentation. These experimental parameters led to 48%, and 61% of sequence coverage of the sdADC, respectively (**Figure S9**), increasing significantly the sequence coverage obtained with HCD, as expected (**Figure 3**).

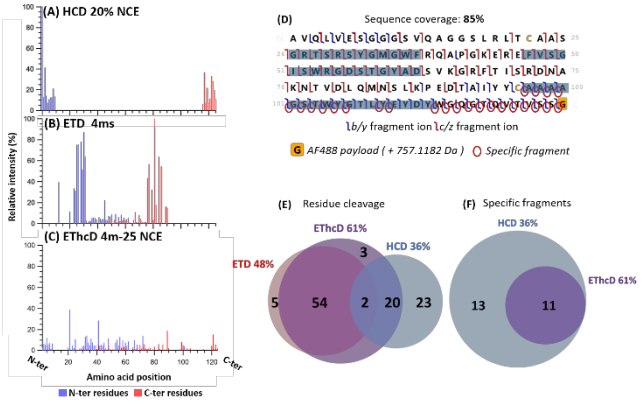

Figure 3: Location of C-terminal and N-terminal fragments upon sdADC fragmentation using (**A**) 20% NCE HCD, (**B**) 4 ms ETD and (**C**) 4 ms-25% NCE for EThcD. (**D**) Total sequence coverage after combination of the three results. All the included fragments were obtained in at least two out of three replicates. AF488 modification is outlined with an orange frame and specific fragments are depicted in red circles. (**E**) Residue cleavage of the different fragmentation techniques with shared and unique fragments. (**F**) Number of specific fragments to the C-terminal modification upon HCD, ETD and EThcD. CDRs are highlighted with light blue in the sdADC ion map.

According to the ion maps of ETD, and EThcD fragmentations, the mid regions of the sdADC were efficiently fragmented, especially between the 26, and 76 residues where the sequence coverage was 90%, and 84% for ETD, and EThcD respectively (**Figure S9-S10**). This region was poorly characterized with HCD fragmentation, highlighting the great interest of combining orthogonal fragmentation techniques for an enhanced sequence coverage.[60,68,69] Thus, ETD, and EThcD afforded complementary results in comparison with HCD, with only two fragments shared by the three fragmentation techniques (less than 2%), raising the overall sdADC sequencing to 85% (**Figure 3, and S10**). However, the latter techniques were not very informative regarding the C-terminal side, and hence the conjugation site of the protein. ETD did not afford any specific fragment of the conjugation, and 11 fragments were observed in the case of EThcD. However, these diagnostic ions arised from the supplemented collisional energy of EThcD activation and hence, they were not specific fragments of the radical fragmentation. Of note, in this particular case where the sdADC was modified with a subrogate payload without a linker and a cytotoxic molecule, HCD offered the lowest sequence coverage but it remained the most suitable method to decipher the conjugation site with 24 fragment ions characteristic of the AF488 conjugation at the C-terminal side.

TD-MS fragmentation of intact sdADC for direct evidence of intra-molecular disulfide bond preservation

TD-MS strategies have been also applied to proteins with inter,[47,51,70–72] and intra-disulfide links.[47,51,65,66,71–74] In some cases, different fragmentation techniques were used to disrupt the disulfide bonds of the proteins with the main purpose of increasing the overall fragmentation yield, and hence provide a better primary structure characterization. Even though collisional activation techniques can potentially fragment disulfide bonds,[73,74] electron-driven fragmentation or photo-dissociation techniques have been shown a more marked propensity to disrupt cysteine-linked proteins either by promoting a S-S homolytic fragmentation mechanism (accompanied or not by a hydrogen transfer)[70,75] or breaking the C-S bonds.[37,47,65] These fragmentation mechanisms give rise to diagnostic fragment ions that can be capitalized not only to increase the overall sequence coverage but also, to decipher the disulfide patterns of proteins with intra- and inter-molecular disulfide linkages. Thereby, the different activation methods included in the current study were used to generate specific fragments of the disulfide bond contained within the structure of the sdADC between the two cysteine residues to provide further evidence about the disulfide linkage integrity upon the conjugation process.

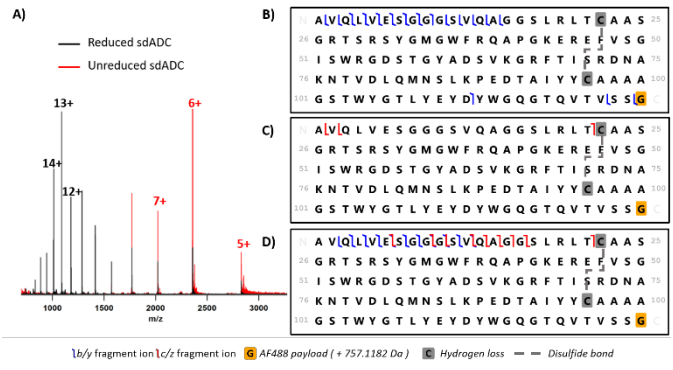

Figure 4: TD-MS experiments of unreduced sdADC. **(A)** Comparison of MS spectra from rpLC-MS analysis of reduced sdADC (black line) *versus* unreduced sdADC (red line) showing the different charge envelopes. **(B)** Fragmentation map upon 30% NCE HCD, (C) 4 ms ETD and **(D)** 4ms and 30% NCE of EThcD. AF488 modification is outlined in orange frame and hydrogen loss modifications are in grey frames. The disulfide bond is depicted in grey dashed line.

The mass spectrum of the non-reduced sdADC clearly shows a dramatic reduction of the overall charge state (**Figure 4A**) compared to the mass spectrum of the reduced sample. The charge state distribution of the reduced sdADC was centered at the 13+ charge state while the most intense species of the non-reduced sample is the 6+ charge state. This is consistent with the fact that almost 60% of the sdADC sequence is flanked by the disulfide bond, leading to a more folded structure which precludes the protonation of the protein, and thus reduces the overall charge state. This characteristic will presumably impair the fragmentation efficiency of the different fragmentation techniques due to both the selection of lower charge state precursor ions, and the hindrance for the internal energy redistribution throughout the whole sdADC sequence. Altogether, the reduced charge state of the precursor ion, the presence of an inter-molecular disulfide bond containing almost 2/3 of the total sequence, and the experimental design aiming at the fragmentation of the sdADC in the LC time scale represent extremely challenging conditions to conduct TD-MS experiments even in the case of a 14 kDa protein.

According to the results, the highest sequence coverage obtained with HCD corresponded to the fragmentation of the 6+ charge state, while the most informative fragmentation spectra for ETD, and EThcD were obtained with the 7+. Overall, the sequence coverage afforded by the three techniques drastically decreased compared to the reduced sdADC. Only three fragment ions were detected upon ETD activation highlighting the limited efficiency of radical fragmentation for low-charged precursor ions. HCD, and EThcD methods provided fragments on the protein regions that were not enclosed by the S-S bond, covering mainly the N-terminus of the sdADC with a series of *y/b*-(HCD), and *c/z*-ion fragments (EThcD) (**Figure 4B, D and S11, 12**). In both cases, *y*-, and *c*-ions corresponded to terminal fragment ions with both cysteine residues in their oxidized form (*i.e.* involved in the intra-molecular bond), and the AF488 moiety conjugated in the C-terminal site of the nanobody, thus corroborating the presence of the disulfide bond and the conjugation site simultaneously. In the particular case of HCD, the b_{112} ion was also identified, providing an additional confirmation about the presence of the disulfide bond with C-, and N-terminal fragments simultaneously. Interestingly HCD, and EThcD provided golden-pair fragments in 35%, and 81% of the total cleaved sites, respectively, strengthen the confidence on fragment ion identification. In spite of the marked selectivity of ETD fragmentation to excise disulfide bonds, hallmarks of disulfide bond cleavage could not be found upon ETD, and EThcD activations (nor with HCD).

In order to dig deeper on the identification of produced fragments from the intact sdADC, fragment ion search space was extended to internal fragments. Therefore, ClipsMS[76] was used to identify fragment ions resulting from multiple protein backbone fragmentation events. The inclusion of internal fragments in the ion searching has been shown beneficial in terms of overall sequence coverage of cysteine-rich proteins, providing an extensive primary sequence characterization.[40,66,73,74] However, internal fragment ion search entails an increasing false positive rate as reported previously in the literature,[33,58] suggesting the use of more stringent fragment mass tolerance, perform a manual validation of the isotopic profile of the fragment, and, when possible, conduct further fragmentation stages for a more confident ion assignment.[74,77]

In the particular case of the sdADC, these ions were exclusively used to identify fragments ions related with the presence of the disulfide bond, *i.e.* either containing both cysteine residues oxidized, or fragments resulting from the dissociation of the disulfide bond. After manual validation, no internal fragments could be confirmed for none of the fragmentation techniques that contained the disulfide bond or specific fragments characteristic of its fragmentation. . Conversely, several internal fragments were identified arising from multiple fragmentation events of the se-

quence region flanked by the disulfide bond (between the 22nd, and 96th peptide bond positions) (**Figure 5**). This result is consistent with previous observations showing that internal fragments are more easily formed than terminal fragments from sequence regions that are highly constrained by intra-molecular disulfide bonds.[66]

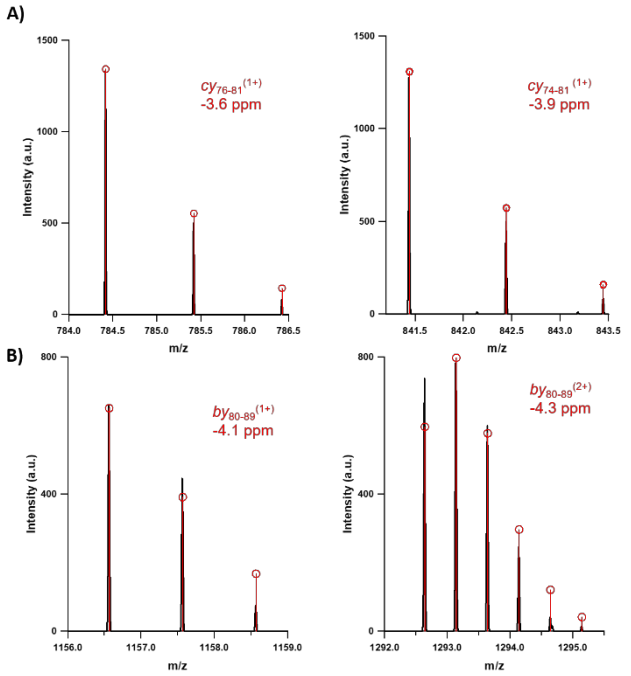

Figure 5: Internal fragment ion matching of intact sdADC. **(A)** Isotopic profile of two internal fragments generated with EThcD 4ms-30% NCE, and (B) HCD 30% NCE activations. The depicted ions correspond to different regions of the sdADC contained within the disulfide bond.

One of the reasons that may lead to the absence of disulfide bond cleavage fragment ions identification stems from the reduced acquisition time of the MS/MS spectra due to the coupling of the LC dimension in the forefront of the mass spectrometer. Most of the studies that envisaged the fragmentation of intact protein with multiple disulfide bonds are conducted in direct infusion, recording the fragmentation spectra during several hundreds of transients.[47,64–66,70,73–75] This is a key parameter that facilitates the identification of low abundant ions by increasing the S/N ratio alongside the acquisition time. This is even more important for diagnostic fragments characteristics of the disulfide bond fragmentation, which relative intensity has been estimated to be less than 5% of the total fragment ion intensity.[64] According to this result, it is highly likely that the reduced acquisition time of the LC-TD-MS spectrum of the sdADC (FWHM 0.11 min) precludes the detection of these low-abundant fragment ions. However, the results recorded with the three fragmentation techniques clearly demonstrate the connectivity of the S-S bond from the Cys22 to the Cys96 residues after confirming the presence of terminal fragments containing both oxidized cysteine residues.

CONCLUSIONS

The current study reports for the first time on the characterization of a sdADC conjugated with a surrogate cytotoxic payload molecule using an optimized LC-TD-MS workflow based on three different activation techniques, *i.e.* HCD, ETD, and EThcD. The results clearly highlight the benefits and limitations of all the three techniques in terms of sequence coverage, conjugation site, and determination/fragmentation of intramolecular disulfide bonds in order to afford the most comprehensive characterization of the sdADC primary structure.

Upon unveiling the number of conjugated molecules attached to the sdAb sequence, the conjugated protein was interrogated with the three different activation methods. As expected by previous analyses, ETD, and EThcD provided extensive sequence characterization, especially in the mid-region of the sdADC. However, HCD fragmentation was more informative regarding the number of fragment ions that were diagnostic to the specific conjugation site. This result seems to disagree with previous studies where electron-dissociation techniques outperformed the results of collisional activation techniques.[33–35] Three main reasons can account for this observation. The first one is that the conjugation site of the sdADC is located in the C-terminal extremity, a region which is normally well sequenced by collisional activation techniques. The second one is that the structure of the cargo molecule used in this study does not contain an ester bond that is commonly used to covalently attach the cytotoxic molecule to the linker of more classical ADC payloads. As a consequence, the AF488 moiety exhibits more resistance to undergo fragmentation, and thus remaining intact upon collisions with the background gas. The last parameter that certainly affects the electron-driven sequence coverage is the lack of basic residues in the C-terminal side of the protein, hampering the transfer of the electrons in this particular part of the sequence, and thus limiting the number of fragments containing the conjugated moiety.

The LC-TD-MS workflow was also applied to the non-reduced sdADC sample to determine the presence of the intramolecular S-S bond after conjugation of the AF488 molecule. The fragmentation efficiency of the three techniques drastically decreased since the disulfide bond stabilizes the secondary structure of the protein leading to a more

compact, and less charged entity. The overall sequence coverage was 16% upon combination of the three techniques. Only a limited number of fragment ions characteristics of the disulfide bond cleavage were identified upon HCD, and EThcD fragmentations. The vast majority of fragment ions stemmed from the fragmentation of the regions near the N-terminal side that were not encompassed by the intra-molecular bond suggesting that the C-terminal extremity is less exposed (or more protected) when the disulfide bond of the sdADC is not reduced. Nevertheless, these ions corroborated the presence of the disulfide bridge along with the localization of the AF488 molecule in the C-terminal side.

Altogether, these results put in evidence that despite the relatively low molecular weight, and the limited structural heterogeneity, the fragmentation and comprehensive characterization of sdAb, and sdADCs at the intact level is still challenge, especially when TD-MS experimental workflows are conducted in the chromatography time scale. However, the use of complementary activation techniques can boost the performances of these workflows in terms of sequence coverage and signature fragment ions, spurring their application to the characterization of a large array of proteins.

ASSOCIATED CONTENT

Supporting Information

The Supporting Information is available free of charge on the ACS Publications website.

Figure S1: SEC-UV chromatogram of cysteamine labelled anti-EGFR VHH. **Figure S2**: Native MS spectra corresponding to the peak at 4.50 min. **Figure S3**: SDS-PAGE gel revealing the resulted products from the anti-EGFR VHH labelling. **Figure S4**: Optimization of the choice of the precursor ion and the HCD NCE. **Figure S5:** Fragmentation maps of sdADC upon 20% NCE HCD. **Figure S6**: Peptide mapping results showing the MS/MS spectra bearing the modification. **Figure S7**: Optimization of the choice of the precursor ion and the reaction time with ETD. **Figure S8**: Optimization of the HCD NCE with EThcD. **Figure S9**: MS/MS spectra showing the obtained fragmentation patterns of the sdADC. **Figure S10**: Fragmentation map obtained via fragmentation of sdAb (left) and sdADC (right). **Figure S11**: Isotopic profiles of fragments from HCD 30% on 6+. **Figure S12**: Isotopic profiles of fragments from EThcD 4 ms - 30% NCE on 7+.

AUTHOR INFORMATION

Corresponding Author

* **Oscar Hernandez-Alba** – Laboratoire de Spectrométrie de masse BioOrganique, Université de Strasbourg, CNRS, IPHC UMR 7178, 67000 Strasbourg, France.
Email : ahernandez@unistra.fr

Authors

†**Rania Benazza -** Laboratoire de Spectrométrie de Masse BioOrganique, IPHC UMR 7178, Université de Strasbourg, CNRS, 67087 Strasbourg, France

†**Léa Letissier -** Laboratoire de Spectrométrie de Masse BioOrganique, IPHC UMR 7178, Université de Strasbourg, CNRS, 67087 Strasbourg, France

Greg Papadokus - Almac discovery, Edinburgh Technopole, Milton Bridge, Penicuik, Scotland, EH26 0BE, United Kingdom

Jen Thom - Almac discovery, Edinburgh Technopole, Milton Bridge, Penicuik, Scotland, EH26 0BE, United Kingdom

Hélène Diemer - Laboratoire de Spectrométrie de Masse BioOrganique, IPHC UMR 7178, Université de Strasbourg, CNRS, 67087 Strasbourg, France

Graham Cotton - Almac discovery, Edinburgh Technopole, Milton Bridge, Penicuik, Scotland, EH26 0BE, United Kingdom

Sarah Cianférani - Laboratoire de Spectrométrie de Masse BioOrganique, IPHC UMR 7178, Université de Strasbourg, CNRS, 67087 Strasbourg, France

Author Contributions

RB, and LL equally contributed to this study. The manuscript was written through contributions of all authors. / All authors have given approval to the final version of the manuscript.

ACKNOWLEDGMENT

This study was supported by the European Union's Horizon
2020 Research and Innovation Programme Marie Sklodowska Curie Action ITN under Grant Agreement No. 859458 (I. K., B. J.,
R. B.), the CNRS, the University of Strasbourg, the "Agence Nationale de la Recherche", and the French Proteomic Infrastructure (ProFI; ANR-10-INBS-08-03). Authors would like to thank the Région Grand-Est (Fonds Régional de la Coopération pour la Recherche, HRMS-INFECT project) in purchasing an Orbitrap Eclipse™ Tribrid™ (Thermo Fisher Scientific) mass spectrometer. LL acknowledges the French Ministry of Higher Education and Research for the PhD fellowship funding. OHA acknowledge the "Agence National de la Recherche" for funding his JCJC project (ConformAbs, ANR-21-CE29-0009-01).

REFERENCES

(1) Crescioli, S.; Kaplon, H.; Chenoweth, A.; Wang, L.; Visweswaraiah, J.; Reichert, J. M. Antibodies to Watch in 2024. *mAbs* **2024**, *16* (1), 2297450. https://doi.org/10.1080/19420862.2023.2297450.

(2) Jin, B. K.; Odongo, S.; Radwanska, M.; Magez, S. Nanobodies: A Review of Generation, Diagnostics and Therapeutics. *Int J Mol Sci* **2023**, *24* (6). https://doi.org/10.3390/ijms24065994.
(3) Yong Joon Kim, J.; Sang, Z.; Xiang, Y.; Shen, Z.; Shi, Y. Nanobodies: Robust Miniprotein Binders in Biomedicine. *Adv Drug Deliv Rev* **2023**, *195*, 114726. https://doi.org/10.1016/j.addr.2023.114726.
(4) Hamers-Casterman, C.; Atarhouch, T.; Muyldermans, S.; Robinson, G.; Hammers, C.; Songa, E. B.; Bendahman, N.; Hammers, R. Naturally Occurring Antibodies Devoid of Light Chains. *Nature* **1993**, *363* (6428), 446–448. https://doi.org/10.1038/363446a0.
(5) Kijanka, M.; Dorresteijn, B.; Oliveira, S.; van Bergen en Henegouwen, P. M. Nanobody-Based Cancer Therapy of Solid Tumors. *Nanomedicine Lond* **2015**, *10* (1), 161–174. https://doi.org/10.2217/nnm.14.178.
(6) Wang, L.; Zhang, G.; Qin, L.; Ye, H.; Wang, Y.; Long, B.; Jiao, Z. Anti-EGFR Binding Nanobody Delivery System to Improve the Diagnosis and Treatment of Solid Tumours. *Recent Pat Anticancer Drug Discov* **2020**, *15* (3), 200–211. https://doi.org/10.2174/1574892815666200904111728.
(7) Bélanger, K.; Iqbal, U.; Tanha, J.; MacKenzie, R.; Moreno, M.; Stanimirovic, D. Single-Domain Antibodies as Therapeutic and Imaging Agents for the Treatment of CNS Diseases. *Antibodies Basel* **2019**, *8* (2). https://doi.org/10.3390/antib8020027.
(8) Pothin, E.; Lesuisse, D.; Lafaye, P. Brain Delivery of Single-Domain Antibodies: A Focus on VHH and VNAR. *Pharmaceutics* **2020**, *12* (10). https://doi.org/10.3390/pharmaceutics12100937.
(9) Henry, K. A.; MacKenzie, C. R. Antigen Recognition by Single-Domain Antibodies: Structural Latitudes and Constraints. *mAbs* **2018**, *10* (6), 815–826. https://doi.org/10.1080/19420862.2018.1489633.
(10) De Genst, E.; Silence, K.; Decanniere, K.; Conrath, K.; Loris, R.; Kinne, J.; Muyldermans, S.; Wyns, L. Molecular Basis for the Preferential Cleft Recognition by Dromedary Heavy-Chain Antibodies. *Proc. Natl. Acad. Sci. U. S. A.* **2006**, *103* (12), 4586–4591. https://doi.org/10.1073/pnas.0505379103.
(11) Ackaert, C.; Smiejkowska, N.; Xavier, C.; Sterckx, Y. G. J.; Denies, S.; Stijlemans, B.; Elkrim, Y.; Devoogdt, N.; Caveliers, V.; Lahoutte, T.; Muyldermans, S.; Breckpot, K.; Keyaerts, M. Immunogenicity Risk Profile of Nanobodies. *Front Immunol* **2021**, *12*, 632687. https://doi.org/10.3389/fimmu.2021.632687.
(12) Rossotti, M. A.; Bélanger, K.; Henry, K. A.; Tanha, J. Immunogenicity and Humanization of Single-Domain Antibodies. *Febs J* **2022**, *289* (14), 4304–4327. https://doi.org/10.1111/febs.15809.
(13) Wang, Y.; Fan, Z.; Shao, L.; Kong, X.; Hou, X.; Tian, D.; Sun, Y.; Xiao, Y.; Yu, L. Nanobody-Derived Nanobiotechnology Tool Kits for Diverse Biomedical and Biotechnology Applications. *Int J Nanomedicine* **2016**, *11*, 3287–3303. https://doi.org/10.2147/ijn.s107194.
(14) Dumoulin, M.; Conrath, K.; Van Meirhaeghe, A.; Meersman, F.; Heremans, K.; Frenken, L. G.; Muyldermans, S.; Wyns, L.; Matagne, A. Single-Domain Antibody Fragments with High Conformational Stability. *Protein Sci. Publ. Protein Soc.* **2002**, *11* (3), 500–515. https://doi.org/10.1110/ps.34602.
(15) Ruano-Gallego, D.; Fraile, S.; Gutierrez, C.; Fernández, L. Á. Screening and Purification of Nanobodies from E. Coli Culture Supernatants Using the Hemolysin Secretion System. *Microb. Cell Factories* **2019**, *18* (1), 47. https://doi.org/10.1186/s12934-019-1094-0.
(16) Gorlani, A.; de Haard, H.; Verrips, T. Expression of VHHs in Saccharomyces Cerevisiae. *Methods Mol Biol* **2012**, *911*, 277–286. https://doi.org/10.1007/978-1-61779-968-6_17.
(17) Mei, Y.; Chen, Y.; Sivaccumar, J. P.; An, Z.; Xia, N.; Luo, W. Research Progress and Applications of Nanobody in Human Infectious Diseases. *Front Pharmacol* **2022**, *13*, 963978. https://doi.org/10.3389/fphar.2022.963978.
(18) Liu, M.; Li, L.; Jin, D.; Liu, Y. Nanobody-A Versatile Tool for Cancer Diagnosis and Therapeutics. *Wiley Interdiscip Rev Nanomed Nanobiotechnol* **2021**, *13* (4), e1697. https://doi.org/10.1002/wnan.1697.
(19) Gao, Y.; Zhu, J.; Lu, H. Single Domain Antibody-Based Vectors in the Delivery of Biologics across the Blood-Brain Barrier: A Review. *Drug Deliv Transl Res* **2021**, *11* (5), 1818–1828. https://doi.org/10.1007/s13346-020-00873-7.
(20) Pronk, S. D.; Schooten, E.; Heinen, J.; Helfrich, E.; Oliveira, S.; van Bergen En Henegouwen, P. M. P. Single Domain Antibodies as Carriers for Intracellular Drug Delivery: A Proof of Principle Study. *Biomolecules* **2021**, *11* (7). https://doi.org/10.3390/biom11070927.
(21) Barakat, S.; Berksöz, M.; Zahedimaram, P.; Piepoli, S.; Erman, B. Nanobodies as Molecular Imaging Probes. *Free Radic Biol Med* **2022**, *182*, 260–275. https://doi.org/10.1016/j.freeradbiomed.2022.02.031.
(22) Brown, K. A.; Tucholski, T.; Alpert, A. J.; Eken, C.; Wesemann, L.; Kyrvasilis, A.; Jin, S.; Ge, Y. Top-Down Proteomics of Endogenous Membrane Proteins Enabled by Cloud Point Enrichment and Multidimensional Liquid Chromatography-Mass Spectrometry. *Anal. Chem.* **2020**, *92* (24), 15726–15735. https://doi.org/10.1021/acs.analchem.0c02533.

(23) Juliano, B. R.; Keating, J. W.; Ruotolo, B. T. Infrared Photoactivation Enables Improved Native Top-Down Mass Spectrometry of Transmembrane Proteins. *Anal. Chem.* **2023**, *95* (35), 13361–13367. https://doi.org/10.1021/acs.analchem.3c02788.

(24) Lutomski, C. A.; El-Baba, T. J.; Hinkle, J. D.; Liko, I.; Bennett, J. L.; Kalmankar, N. V.; Dolan, A.; Kirschbaum, C.; Greis, K.; Urner, L. H.; Kapoor, P.; Yen, H. Y.; Pagel, K.; Mullen, C.; Syka, J. E. P.; Robinson, C. V. Infrared Multiphoton Dissociation Enables Top-Down Characterization of Membrane Protein Complexes and G Protein-Coupled Receptors. *Angew. Chem. Int. Ed. Engl.* **2023**, *62* (36), e202305694. https://doi.org/10.1002/anie.202305694.

(25) Gault, J.; Liko, I.; Landreh, M.; Shutin, D.; Bolla, J. R.; Jefferies, D.; Agasid, M.; Yen, H. Y.; Ladds, M.; Lane, D. P.; Khalid, S.; Mullen, C.; Remes, P. M.; Huguet, R.; McAlister, G.; Goodwin, M.; Viner, R.; Syka, J. E. P.; Robinson, C. V. Combining Native and "omics" Mass Spectrometry to Identify Endogenous Ligands Bound to Membrane Proteins. *Nat Methods* **2020**, *17* (5), 505–508. https://doi.org/10.1038/s41592-020-0821-0.

(26) Walker, J. N.; Lam, R.; Brodbelt, J. S. Enhanced Characterization of Histones Using 193 Nm Ultraviolet Photodissociation and Proton Transfer Charge Reduction. *Anal. Chem.* **2023**, *95* (14), 5985–5993. https://doi.org/10.1021/acs.analchem.2c05765.

(27) Berthias, F.; Thurman, H. A.; Wijegunawardena, G.; Wu, H.; Shvartsburg, A. A.; Jensen, O. N. Top-Down Ion Mobility Separations of Isomeric Proteoforms. *Anal. Chem.* **2023**, *95* (2), 784–791. https://doi.org/10.1021/acs.analchem.2c02948.

(28) Jeanne Dit Fouque, K.; Miller, S. A.; Pham, K.; Bhanu, N. V.; Cintron-Diaz, Y. L.; Leyva, D.; Kaplan, D.; Voinov, V. G.; Ridgeway, M. E.; Park, M. A.; Garcia, B. A.; Fernandez-Lima, F. Top-"Double-Down" Mass Spectrometry of Histone H4 Proteoforms: Tandem Ultraviolet-Photon and Mobility/Mass-Selected Electron Capture Dissociations. *Anal. Chem.* **2022**, *94* (44), 15377–15385. https://doi.org/10.1021/acs.analchem.2c03147.

(29) Peters-Clarke, T. M.; Quan, Q.; Brademan, D. R.; Hebert, A. S.; Westphall, M. S.; Coon, J. J. Ribonucleic Acid Sequence Characterization by Negative Electron Transfer Dissociation Mass Spectrometry. *Anal. Chem.* **2020**, *92* (6), 4436–4444. https://doi.org/10.1021/acs.analchem.9b05388.

(30) Santos, I. C.; Lanzillotti, M.; Shilov, I.; Basanta-Sanchez, M.; Roushan, A.; Lawler, R.; Tang, W.; Bern, M.; Brodbelt, J. S. Ultraviolet Photodissociation and Activated Electron Photodetachment Mass Spectrometry for Top-Down Sequencing of Modified Oligoribonucleotides. *J. Am. Soc. Mass Spectrom.* **2022**, *33* (3), 510–520. https://doi.org/10.1021/jasms.1c00340.

(31) Crittenden, C. M.; Lanzillotti, M. B.; Chen, B. Top-Down Mass Spectrometry of Synthetic Single Guide Ribonucleic Acids Enabled by Facile Sample Clean-Up. *Anal. Chem.* **2023**, *95* (6), 3180–3186. https://doi.org/10.1021/acs.analchem.2c03030.

(32) Dhenin, J.; Dupré, M.; Druart, K.; Krick, A.; Mauriac, C.; Chamot-Rooke, J. A Multiparameter Optimization in Middle-down Analysis of Monoclonal Antibodies by LC-MS/MS. *J. Mass Spectrom.* **2023**, *58* (3), e4909. https://doi.org/10.1002/jms.4909.

(33) Beaumal, C.; Deslignière, E.; Diemer, H.; Carapito, C.; Cianférani, S.; Hernandez-Alba, O. Improved Characterization of Trastuzumab Deruxtecan with PTCR and Internal Fragments Implemented in Middle-down MS Workflows. *Anal. Bioanal. Chem.* **2023**. https://doi.org/10.1007/s00216-023-05059-x.

(34) Watts, E.; Williams, J. D.; Miesbauer, L. J.; Bruncko, M.; Brodbelt, J. S. Comprehensive Middle-Down Mass Spectrometry Characterization of an Antibody-Drug Conjugate by Combined Ion Activation Methods. *Anal. Chem.* **2020**, *92* (14), 9790–9798. https://doi.org/10.1021/acs.analchem.0c01232.

(35) Hernandez-Alba, O.; Houel, S.; Hessmann, S.; Erb, S.; Rabuka, D.; Huguet, R.; Josephs, J.; Beck, A.; Drake, P. M.; Cianférani, S. A Case Study to Identify the Drug Conjugation Site of a Site-Specific Antibody-Drug-Conjugate Using Middle-Down Mass Spectrometry. *J. Am. Soc. Mass Spectrom.* **2019**, *30* (11), 2419–2429. https://doi.org/10.1007/s13361-019-02296-2.

(36) Chen, B.; Lin, Z.; Zhu, Y.; Jin, Y.; Larson, E.; Xu, Q.; Fu, C.; Zhang, Z.; Zhang, Q.; Pritts, W. A.; Ge, Y. Middle-Down Multi-Attribute Analysis of Antibody-Drug Conjugates with Electron Transfer Dissociation. *Anal. Chem.* **2019**, *91* (18), 11661–11669. https://doi.org/10.1021/acs.analchem.9b02194.

(37) Srzentic, K.; Nagornov, K. O.; Fornelli, L.; Lobas, A. A.; Ayoub, D.; Kozhinov, A. N.; Gasilova, N.; Menin, L.; Beck, A.; Gorshkov, M. V.; Aizikov, K.; Tsybin, Y. O. Multiplexed Middle-Down Mass Spectrometry as a Method for Revealing Light and Heavy Chain Connectivity in a Monoclonal Antibody. *Anal. Chem.* **2018**, *90* (21), 12527–12535. https://doi.org/10.1021/acs.analchem.8b02398.

(38) Cotham, V. C.; Brodbelt, J. S. Characterization of Therapeutic Monoclonal Antibodies at the Subunit-Level Using Middle-Down 193 Nm Ultraviolet Photodissociation. *Anal. Chem.* **2016**, *88* (7), 4004–4013. https://doi.org/10.1021/acs.analchem.6b00302.

(39) Fornelli, L.; Ayoub, D.; Aizikov, K.; Beck, A.; Tsybin, Y. O. Middle-Down Analysis of Monoclo-

nal Antibodies with Electron Transfer Dissociation Orbitrap Fourier Transform Mass Spectrometry. *Anal. Chem.* **2014**, *86* (6), 3005–3012. https://doi.org/10.1021/ac4036857.

(40) Wei, B.; Lantz, C.; Ogorzalek Loo, R. R.; Campuzano, I. D. G.; Loo, J. A. Internal Fragments Enhance Middle-Down Mass Spectrometry Structural Characterization of Monoclonal Antibodies and Antibody-Drug Conjugates. *Anal. Chem.* **2024**. https://doi.org/10.1021/acs.analchem.3c04526.

(41) Melani, R. D.; Srzentić, K.; Gerbasi, V. R.; McGee, J. P.; Huguet, R.; Fornelli, L.; Kelleher, N. L. Direct Measurement of Light and Heavy Antibody Chains Using Ion Mobility and Middle-down Mass Spectrometry. *mAbs* **2019**, *11* (8), 1351–1357. https://doi.org/10.1080/19420862.2019.1668226.

(42) Fornelli, L.; Damoc, E.; Thomas, P. M.; Kelleher, N. L.; Aizikov, K.; Denisov, E.; Makarov, A.; Tsybin, Y. O. Analysis of Intact Monoclonal Antibody IgG1 by Electron Transfer Dissociation Orbitrap FTMS. *Mol. Cell. Proteomics* **2012**, *11* (12), 1758–1767. https://doi.org/10.1074/mcp.M112.019620.

(43) Tsybin, Y. O.; Fornelli, L.; Stoermer, C.; Luebeck, M.; Parra, J.; Nallet, S.; Wurm, F. M.; Hartmer, R. Structural Analysis of Intact Monoclonal Antibodies by Electron Transfer Dissociation Mass Spectrometry. *Anal. Chem.* **2011**, *83* (23), 8919–8927. https://doi.org/10.1021/ac201293m.

(44) Fornelli, L.; Ayoub, D.; Aizikov, K.; Liu, X. W.; Damoc, E.; Pevzner, P. A.; Makarov, A.; Beck, A.; Tsybin, Y. O. Top-down Analysis of Immunoglobulin G Isotypes 1 and 2 with Electron Transfer Dissociation on a High-Field Orbitrap Mass Spectrometer. *J Proteomics* **2017**, *159*, 67–76. https://doi.org/10.1016/j.jprot.2017.02.013.

(45) Mao, Y.; Valeja, S. G.; Rouse, J. C.; Hendrickson, C. L.; Marshall, A. G. Top-Down Structural Analysis of an Intact Monoclonal Antibody by Electron Capture Dissociation-Fourier Transform Ion Cyclotron Resonance-Mass Spectrometry. *Anal. Chem.* **2013**, *85* (9), 4239–4246. https://doi.org/10.1021/ac303525n.

(46) Lodge, J. M.; Schauer, K. L.; Brademan, D. R.; Riley, N. M.; Shishkova, E.; Westphall, M. S.; Coon, J. J. Top-Down Characterization of an Intact Monoclonal Antibody Using Activated Ion Electron Transfer Dissociation. *Anal. Chem.* **2020**, *92* (15), 10246–10251. https://doi.org/10.1021/acs.analchem.0c00705.

(47) Shaw, J. B.; Liu, W.; Vasil Ev, Y. V.; Bracken, C. C.; Malhan, N.; Guthals, A.; Beckman, J. S.; Voinov, V. G. Direct Determination of Antibody Chain Pairing by Top-down and Middle-down Mass Spectrometry Using Electron Capture Dissociation and Ultraviolet Photodissociation. *Anal. Chem.* **2020**, *92* (1), 766–773. https://doi.org/10.1021/acs.analchem.9b03129.

(48) Srzentić, K.; Fornelli, L.; Tsybin, Y. O.; Loo, J. A.; Seckler, H.; Agar, J. N.; Anderson, L. C.; Bai, D. L.; Beck, A.; Brodbelt, J. S.; van der Burgt, Y. E. M.; Chamot-Rooke, J.; Chatterjee, S.; Chen, Y.; Clarke, D. J.; Danis, P. O.; Diedrich, J. K.; D'Ippolito, R. A.; Dupré, M.; Gasilova, N.; Ge, Y.; Goo, Y. A.; Goodlett, D. R.; Greer, S.; Haselmann, K. F.; He, L.; Hendrickson, C. L.; Hinkle, J. D.; Holt, M. V.; Hughes, S.; Hunt, D. F.; Kelleher, N. L.; Kozhinov, A. N.; Lin, Z.; Malosse, C.; Marshall, A. G.; Menin, L.; Millikin, R. J.; Nagornov, K. O.; Nicolardi, S.; Paša-Tolić, L.; Pengelley, S.; Quebbemann, N. R.; Resemann, A.; Sandoval, W.; Sarin, R.; Schmitt, N. D.; Shabanowitz, J.; Shaw, J. B.; Shortreed, M. R.; Smith, L. M.; Sobott, F.; Suckau, D.; Toby, T.; Weisbrod, C. R.; Wildburger, N. C.; Yates, J. R.; Yoon, S. H.; Young, N. L.; Zhou, M. Interlaboratory Study for Characterizing Monoclonal Antibodies by Top-Down and Middle-Down Mass Spectrometry. *J. Am. Soc. Mass Spectrom.* **2020**, *31* (9), 1783–1802. https://doi.org/10.1021/jasms.0c00036.

(49) Fornelli, L.; Srzentić, K.; Huguet, R.; Mullen, C.; Sharma, S.; Zabrouskov, V.; Fellers, R. T.; Durbin, K. R.; Compton, P. D.; Kelleher, N. L. Accurate Sequence Analysis of a Monoclonal Antibody by Top-Down and Middle-Down Orbitrap Mass Spectrometry Applying Multiple Ion Activation Techniques. *Anal. Chem.* **2018**, *90* (14), 8421–8429. https://doi.org/10.1021/acs.analchem.8b00984.

(50) Oates, R. N.; Lieu, L. B.; Srzentić, K.; Damoc, E.; Fornelli, L. Characterization of a Monoclonal Antibody by Native and Denaturing Top-Down Mass Spectrometry. *J. Am. Soc. Mass Spectrom.* **2024**, *35* (9), 2197–2208. https://doi.org/10.1021/jasms.4c00224.

(51) Wei, B.; Lantz, C.; Liu, W.; Viner, R.; Ogorzalek Loo, R. R.; Campuzano, I. D. G.; Loo, J. A. Added Value of Internal Fragments for Top-Down Mass Spectrometry of Intact Monoclonal Antibodies and Antibody–Drug Conjugates. *Anal. Chem.* **2023**. https://doi.org/10.1021/acs.analchem.3c01426.

(52) Larson, E. J.; Roberts, D. S.; Melby, J. A.; Buck, K. M.; Zhu, Y.; Zhou, S.; Han, L.; Zhang, Q.; Ge, Y. High-Throughput Multi-Attribute Analysis of Antibody-Drug Conjugates Enabled by Trapped Ion Mobility Spectrometry and Top-Down Mass Spectrometry. *Anal. Chem.* **2021**, *93* (29), 10013–10021. https://doi.org/10.1021/acs.analchem.1c00150.

(53) Resemann, A.; Wunderlich, D.; Rothbauer, U.; Warscheid, B.; Leonhardt, H.; Fuchser, J.; Kuhlmann, K.; Suckau, D. Top-down de Novo Protein Sequencing of a 13.6 kDa Camelid Single Heavy Chain Antibody by Matrix-Assisted Laser Desorption Ionization-Time-of-Flight/Time-of-Flight Mass Spectrometry. *Anal. Chem.* **2010**, *82*

(8), 3283–3292. https://doi.org/10.1021/ac1000515.
(54) Macias, L. A.; Wang, X.; Davies, B. W.; Brodbelt, J. S. Mapping Paratopes of Nanobodies Using Native Mass Spectrometry and Ultraviolet Photodissociation. *Chem. Sci.* **2022**, *13* (22), 6610–6618. https://doi.org/10.1039/d2sc01536f.
(55) Gibson, T. J.; Smyth, P.; McDaid, W. J.; Lavery, D.; Thom, J.; Cotton, G.; Scott, C. J.; Themistou, E. Single-Domain Antibody-Functionalized pH-Responsive Amphiphilic Block Copolymer Nanoparticles for Epidermal Growth Factor Receptor Targeted Cancer Therapy. *ACS Macro Lett.* **2018**, *7* (8), 1010–1015. https://doi.org/10.1021/acsmacrolett.8b00461.
(56) Okuda, S.; Watanabe, Y.; Moriya, Y.; Kawano, S.; Yamamoto, T.; Matsumoto, M.; Takami, T.; Kobayashi, D.; Araki, N.; Yoshizawa, A. C.; Tabata, T.; Sugiyama, N.; Goto, S.; Ishihama, Y. jPOSTrepo: An International Standard Data Repository for Proteomes. *Nucleic Acids Res.* **2017**, *45* (D1), D1107–D1111. https://doi.org/10.1093/nar/gkw1080.
(57) Rogers, H. T.; Roberts, D. S.; Larson, E. J.; Melby, J. A.; Rossler, K. J.; Carr, A. V.; Brown, K. A.; Ge, Y. Comprehensive Characterization of Endogenous Phospholamban Proteoforms Enabled by Photocleavable Surfactant and Top-down Proteomics. *Anal. Chem.* **2023**, *95* (35), 13091–13100. https://doi.org/10.1021/acs.analchem.3c01618.
(58) Dunham, S. D.; Wei, B.; Lantz, C.; Loo, J. A.; Brodbelt, J. S. Impact of Internal Fragments on Top-Down Analysis of Intact Proteins by 193 Nm UVPD. *J. Proteome Res.* **2023**, *22* (1), 170–181. https://doi.org/10.1021/acs.jproteome.2c00583.
(59) Brodbelt, J. S. Deciphering Combinatorial Post-Translational Modifications by Top-down Mass Spectrometry. *Curr. Opin. Chem. Biol.* **2022**, *70*, 102180. https://doi.org/10.1016/j.cbpa.2022.102180.
(60) Greer, S. M.; Brodbelt, J. S. Top-Down Characterization of Heavily Modified Histones Using 193 Nm Ultraviolet Photodissociation Mass Spectrometry. *J. Proteome Res.* **2018**, *17* (3), 1138–1145. https://doi.org/10.1021/acs.jproteome.7b00801.
(61) Miller, S. A.; Jeanne Dit Fouque, K.; Hard, E. R.; Balana, A. T.; Kaplan, D.; Voinov, V. G.; Ridgeway, M. E.; Park, M. A.; Anderson, G. A.; Pratt, M. R.; Fernandez-Lima, F. Top/Middle-Down Characterization of α-Synuclein Glycoforms. *Anal. Chem.* **2023**, *95* (49), 18039–18045. https://doi.org/10.1021/acs.analchem.3c02405.
(62) Fornelli, L.; Parra, J.; Hartmer, R.; Stoermer, C.; Lubeck, M.; Tsybin, Y. O. Top-down Analysis of 30-80 kDa Proteins by Electron Transfer Dissociation Time-of-Flight Mass Spectrometry. *Anal. Bioanal. Chem.* **2013**, *405* (26), 8505–8514. https://doi.org/10.1007/s00216-013-7267-5.
(63) Kline, J. T.; Mullen, C.; Durbin, K. R.; Oates, R. N.; Huguet, R.; Syka, J. E. P.; Fornelli, L. Sequential Ion-Ion Reactions for Enhanced Gas-Phase Sequencing of Large Intact Proteins in a Tribrid Orbitrap Mass Spectrometer. *J. Am. Soc. Mass Spectrom.* **2021**, *32* (9), 2334–2345. https://doi.org/10.1021/jasms.1c00062.
(64) Zhang, J.; Ogorzalek Loo, R. R.; Loo, J. A. Increasing Fragmentation of Disulfide-Bonded Proteins for Top-Down Mass Spectrometry by Supercharging. *Int. J. Mass Spectrom.* **2015**, *377*, 546–556. https://doi.org/10.1016/j.ijms.2014.07.047.
(65) Rush, M. J. P.; Riley, N. M.; Westphall, M. S.; Coon, J. J. Top-Down Characterization of Proteins with Intact Disulfide Bonds Using Activated-Ion Electron Transfer Dissociation. *Anal. Chem.* **2018**, *90* (15), 8946–8953. https://doi.org/10.1021/acs.analchem.8b01113.
(66) Wei, B.; Zenaidee, M. A.; Lantz, C.; Williams, B. J.; Totten, S.; Ogorzalek Loo, R. R.; Loo, J. A. Top-down Mass Spectrometry and Assigning Internal Fragments for Determining Disulfide Bond Positions in Proteins. *Analyst* **2022**, *148* (1), 26–37. https://doi.org/10.1039/d2an01517j.
(67) Juetten, K. J.; Brodbelt, J. S. Top-Down Analysis of Supercharged Proteins Using Collision-, Electron-, and Photon-Based Activation Methods. *J. Am. Soc. Mass Spectrom.* **2023**, *34* (7), 1467–1476. https://doi.org/10.1021/jasms.3c00138.
(68) Oates, R. N.; Lieu, L. B.; Kline, J. T.; Mullen, C.; Srzentić, K.; Huguet, R.; McAlister, G. C.; Huang, J.; Bergen, D.; Melani, R. D.; Zabrouskov, V.; Durbin, K. R.; Syka, J. E. P.; Fornelli, L. Towards a Universal Method for Middle-down Analysis of Antibodies via Proton Transfer Charge Reduction—Orbitrap Mass Spectrometry. *Anal. Bioanal. Chem.* **2024**, *416* (28), 6463–6472. https://doi.org/10.1007/s00216-024-05534-z.
(69) Kline, J. T.; Huang, J.; Lieu, L. B.; Srzentić, K.; Bergen, D.; Mullen, C.; McAlister, G. C.; Durbin, K. R.; Melani, R. D.; Fornelli, L. Top-down Mass Spectrometry Analysis of Capsid Proteins of Recombinant Adeno-Associated Virus Using Multiple Ion Activations and Proton Transfer Charge Reduction. *PROTEOMICS* **2024**, *n/a* (n/a), e2400223. https://doi.org/10.1002/pmic.202400223.
(70) Macias, L. A.; Brodbelt, J. S. Investigation of Product Ions Generated by 193 Nm Ultraviolet Photodissociation of Peptides and Proteins Containing Disulfide Bonds. *J. Am. Soc. Mass Spectrom.* **2022**, *33* (7), 1315–1324. https://doi.org/10.1021/jasms.2c00124.
(71) Gammelgaard, S. K.; Petersen, S. B.; Haselmann, K. F.; Nielsen, P. K. Characterization of Insulin Dimers by Top-Down Mass Spectrometry. *J. Am.*

Soc. Mass Spectrom. **2021**, *32* (8), 1910–1918. https://doi.org/10.1021/jasms.0c00257.

(72) Quick, M. M.; Crittenden, C. M.; Rosenberg, J. A.; Brodbelt, J. S. Characterization of Disulfide Linkages in Proteins by 193 Nm Ultraviolet Photodissociation (UVPD) Mass Spectrometry. *Anal. Chem.* **2018**, *90* (14), 8523–8530. https://doi.org/10.1021/acs.analchem.8b01556.

(73) Chen, J.; Shiyanov, P.; Zhang, L.; Schlager, J. J.; Green-Church, K. B. Top-down Characterization of a Native Highly Intralinked Protein: Concurrent Cleavages of Disulfide and Protein Backbone Bonds. *Anal. Chem.* **2010**, *82* (14), 6079–6089. https://doi.org/10.1021/ac1006766.

(74) Chen, J.; Shiyanov, P.; Schlager, J. J.; Green, K. B. A Pseudo MS3 Approach for Identification of Disulfide-Bonded Proteins: Uncommon Product Ions and Database Search. *J. Am. Soc. Mass Spectrom.* **2012**, *23* (2), 225–243. https://doi.org/10.1007/s13361-011-0294-6.

(75) Zhao, X.; Shen, Y.; Tong, W.; Wang, G.; Chen, D. D. Y. Deducing Disulfide Patterns of Cysteine-Rich Proteins Using Signature Fragments Produced by Top-down Mass Spectrometry. *Analyst* **2018**, *143* (4), 817–823. https://doi.org/10.1039/c7an01625e.

(76) Lantz, C.; Zenaidee, M. A.; Wei, B.; Hemminger, Z.; Ogorzalek Loo, R. R.; Loo, J. A. ClipsMS: An Algorithm for Analyzing Internal Fragments Resulting from Top-Down Mass Spectrometry. *J. Proteome Res.* **2021**, *20* (4), 1928–1935. https://doi.org/10.1021/acs.jproteome.0c00952.

(77) Mikawy, N. N.; Rojas Ramírez, C.; DeFiglia, S. A.; Szot, C. W.; Le, J.; Lantz, C.; Wei, B.; Zenaidee, M. A.; Blakney, G. T.; Nesvizhskii, A. I.; Loo, J. A.; Ruotolo, B. T.; Shabanowitz, J.; Anderson, L. C.; Håkansson, K. Are Internal Fragments Observable in Electron Based Top-Down Mass Spectrometry? *Mol. Cell. Proteomics* **2024**, *23* (9), 100814. https://doi.org/10.1016/j.mcpro.2024.100814.